Low-frequency seismic: the next revolution in resolution

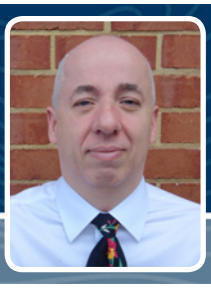

Lead author
Andrew Long

A. Long[1] and C. Reiser[2]
Petroleum Geo-Services (PGS)
[1]IBM Centre
1060 Hay Street
West Perth, WA 6005
[2]4 The Heights
Brooklands, Weybridge
Surrey, KT13 0NY, UK
andrew.long@pgs.com

ABSTRACT

Ultra-low seismic frequencies less than about 7 Hz cannot be produced by conventional air gun arrays, for any configuration and for any towing depth. There is a profound difference between improving low-frequency recovery by removing source and receiver ghosts (achievable) and improving low-frequency injection on the source side (an unrealised dream).

If 1–7 Hz amplitudes could be usefully injected into the earth, it would be possible to facilitate much sharper seismic representation of geological contacts and internal features, and seismic inversion would yield robust and precise predictions of reservoir properties—without well control. The net result is fewer exploration and appraisal wells, greatly reduced exploration and development risks, and optimised recoverable reserves.

Furthermore, an emerging seismic pursuit known as full waveform inversion (FWI) makes the bold promise that raw seismic field gathers can be directly used to invert for the highest achievable velocity models, almost without any human intervention. These models will bypass the traditional lack of low-frequency information in band-limited seismic data, and facilitate the aforementioned ambition of seismic inversion without well control. FWI, however, is confronted by the paradox that ultra-low-frequency seismic gathers are the necessary input for stable results.

This paper describes new technologies that may enable the injection of strong 2–7 Hz amplitudes into the earth, and explains in simple terms how FWI can already be pursued as a robust complement to the prediction of accurate reservoir properties.

The low-frequency revolution is already here.

KEYWORDS

Low-frequency, ghosts, deghosting, dual-sensor, seismic inversion, FWI, reservoir characterisation, seismic.

INTRODUCTION

Conventional air gun source arrays used for towed streamer (marine) seismic surveys cannot produce significant amplitudes below about 7 Hz. This 0–7 Hz range will be referred to as 'ultra-low frequencies'. Although it may be counterintuitive, ultra-low frequency amplitudes can greatly improve vertical (temporal) seismic resolution, as demonstrated in Figure 1. Assuming that equal amplitudes are recovered in processing for all frequencies of relevance, additional low-frequency amplitudes will significantly attenuate sidelobe amplitudes on the zero phase wavelet representing elastic impedance boundaries in the earth. Note also in Figure 1 how additional low-frequency amplitudes do not affect the width of the central event. Overall, the interference between neighbouring reflection events in vertical columns of thin stratified layers will be minimised, thus optimising vertical resolution.

Ultra-low frequency amplitudes are also critical for quantitatively precise estimation of elastic reservoir properties, which will be discussed later. Figure 2 is a comparison of two-dimensional towed streamer results over the Møre Margin area of the Norwegian North Sea. Note how the additional low-frequency amplitudes recovered in the ghost-free data have contributed to reduced sidelobe amplitudes, greatly sharpening the resolution of all events. The sedimentary wedge in the upper right of each panel has smeared resolution on the conventional data, but is crisply resolved in the ghost-free data. Note also how the P-impedance color scale enables the delineation of different lithology classes in the right side of Figure 2.

When describing the so-called penetration of low-frequency amplitudes into the earth it is often the case that two very different scenarios are confused:

1. Injecting stronger low frequencies into the earth; and,
2. recovering low-frequency amplitudes affected by source-side and receiver-side ghost effects.

As will be discussed, the latter scenario is becoming increasingly achievable with modern technological developments, but the former scenario remains frustratingly elusive. The following section defines the phenomena of free-surface ghosts and discusses the limits of low-frequency amplitude recovery through deghosting.

UNWANTED REFLECTIONS FROM THE FREE-SURFACE OF THE OCEAN

Figure 3 illustrates how reflections from the free-surface of the ocean interfere in a continuous and destructive manner with the primary reflections from every interface in the earth. The sedimentary wedge identified in the left side of Figure 2 has elongated and ambiguous seismic events associated with both the top and bottom boundaries of the wedge have occured due to source-side and receiver-side ghosting. Every other geological boundary imaged in the left side of Figure 2 is corrupted in the same manner, but is revealed with often startling clarity in the ghost-free image on the right side of Figure 2. Note in the centre column of Figure 3 how the removal of the receiver-side ghost effects reduces the reflection wavelet from four to two events from each reflecting interface, and in the right column of Figure 3 the additional removal of the source-side ghost effects reduces the reflection wavelet from two events to a single spike. The final processing step in Figure 3 has removed the long-period, low-frequency bubble tail from the data, revealing the ghost-free high resolution image of the earth. The low-frequency content in the bubble energy produced by air guns is discussed later.

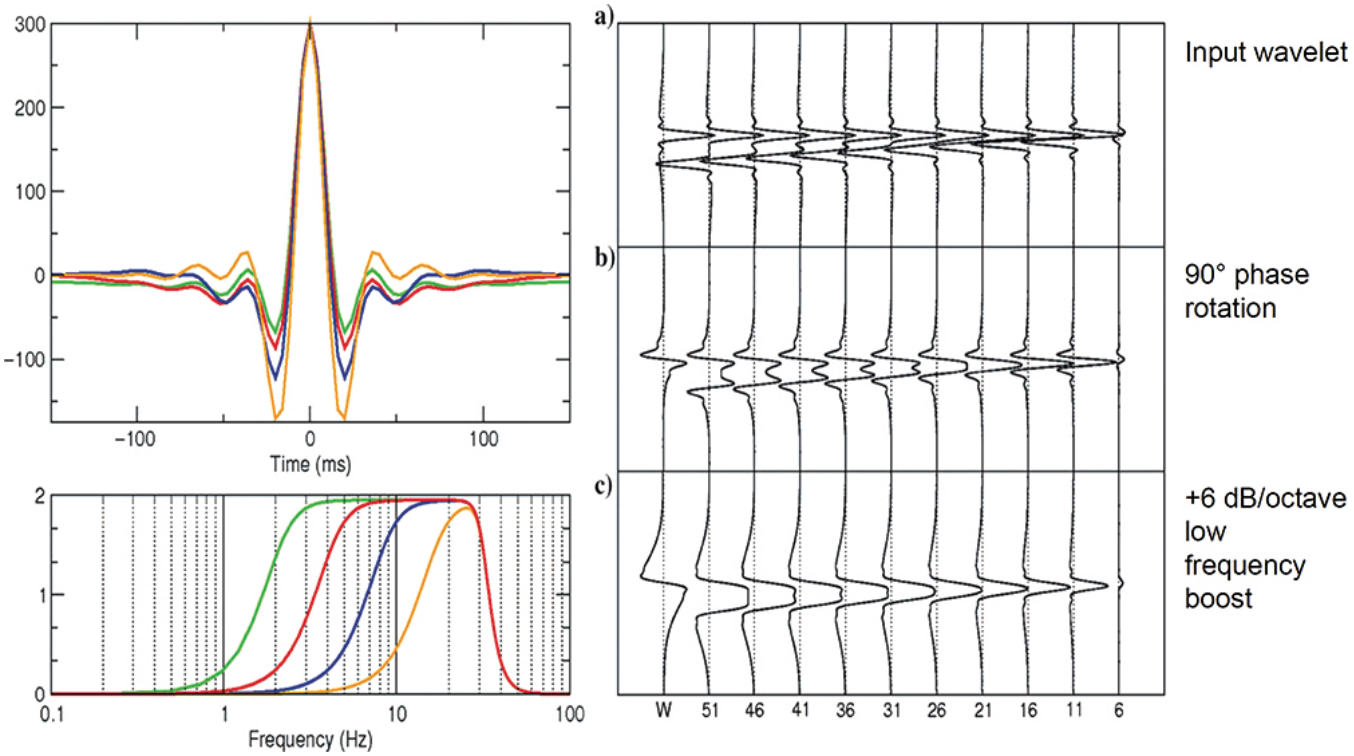

Figure 1. Butterworth filter high cut 32 Hz and 12 dB/octave low cut at 2 (green), 4 (red), 8 (blue), and 16 (yellow) Hz, respectively. The first trace in each panel from the thin wedge modelling is the reflection wavelet from the top of the wedge. Low-frequency boosting suppresses sidelobe interference. From ten Kroode et al (2013), Figure 1.

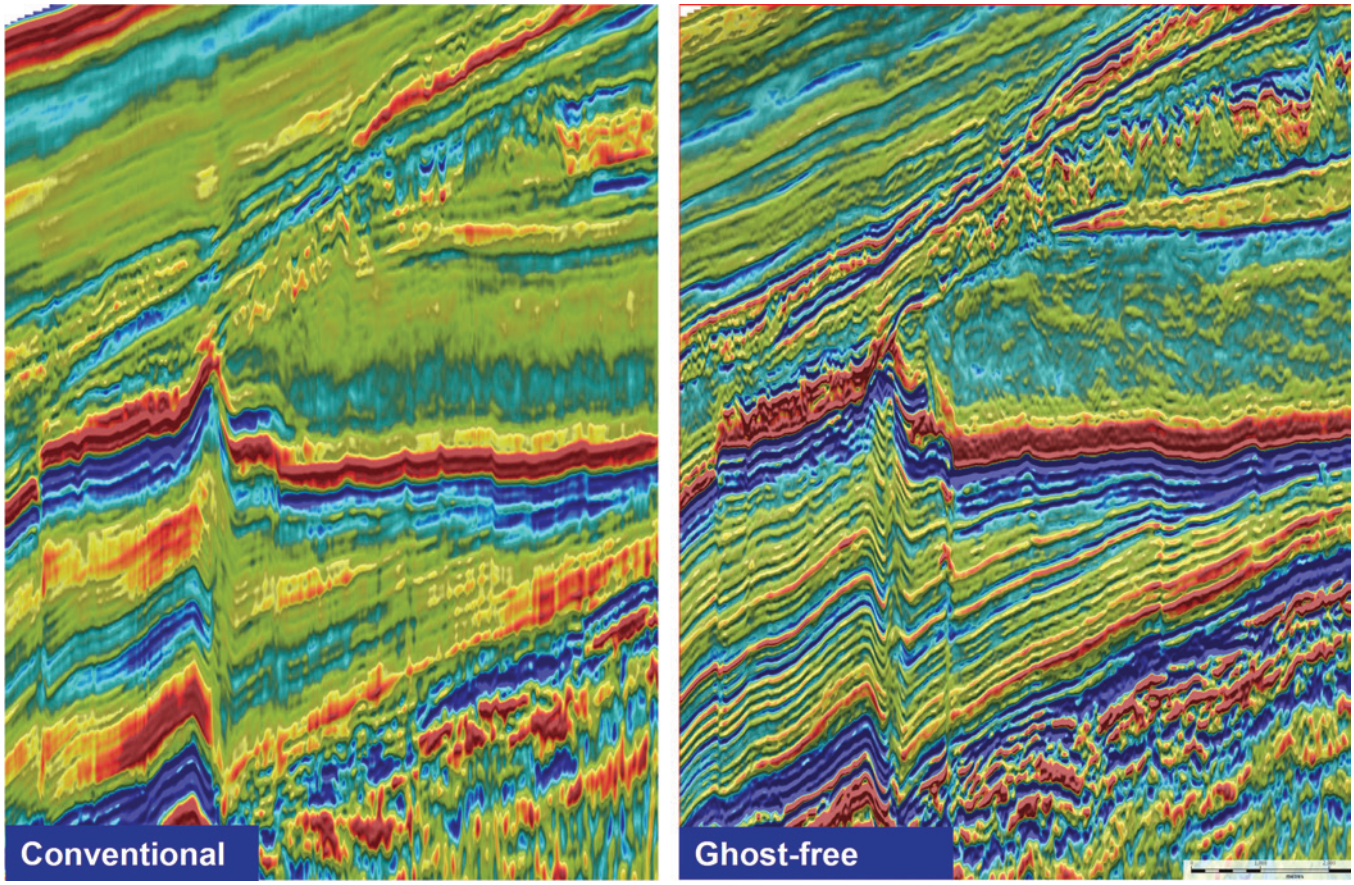

Figure 2. The data on the left were acquired with conventional source and streamer technology, and contain the effects of both the source-side and receiver-side ghost effects (refer also to Fig. 3). In contrast, the data on the right were acquired with acquisition technologies that allow the full removal of both the source-side and receiver-side ghost effects. Note the significantly sharper and more detailed resolution on the right. Both datasets were taken through pre-stack simultaneous seismic inversion. The colour scale represents the relative acoustic impedance (P-impedance), the product of interval velocity and bulk density.

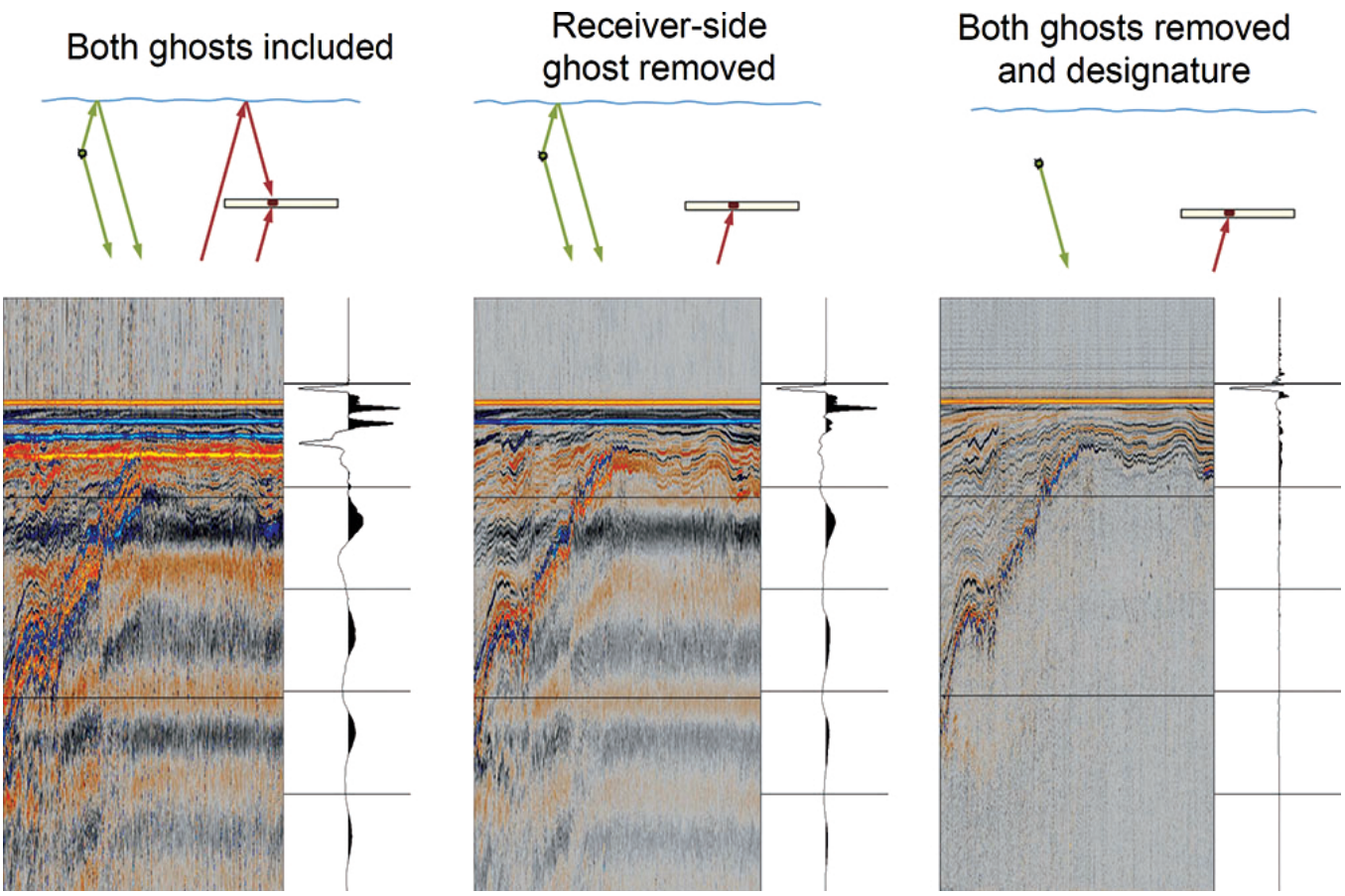

Figure 3. Sequential workflow illustrating the benefits of receiver-side and source-side ghost removal in towed streamer seismic data. The schematic figures along the top row illustrate the universal scenario on the left where four seismic events are in fact recorded from every interface in the earth. In the typical configuration where the streamer is towed deeper than the source array, the sequential order of arrivals recorded is: primary reflection, source-side ghost (opposite polarity), receiver-side ghost (opposite polarity) and both source-side and receiver-side ghost (same polarity as the primary reflection). The single trace in each of the three panels is extracted from the stack. The coda of four events is most obvious at the seafloor because of the pronounced impedance contrast, but this coda in fact cascades down any seismic trace, degrading resolution. The three stack panels have each been flattened on the seafloor event.

Figure 4 illustrates the ultra-low frequency response of the ghost function (Carlson et al, 2007). The phenomenon is comparable on both the source and receiver sides of any towed streamer survey. At the source location the source wavefield is radiated in all directions into the water column. If we think of the wavefield propagation between any specific source and receiver locations (refer to the top row of Fig. 3), two versions of the source wavefield will be propagated into the earth—a version that propagated directly into the earth and a time-delayed version (the source ghost) that is reflected from the free-surface of the ocean with opposite polarity (the reflection coefficient is very close to –1.0). For each specific frequency there will be a depth-dependent attenuation or reinforcement of the source wavefield amplitudes depending upon the phase difference between the two time-delayed wavefields. For larger source depths the periodic peaks and notches in the amplitude spectrum move to lower values, and vice-versa. An additional complication is that the periodic peaks and notches in the amplitude spectrum move to higher values as the source emission angle increases (vertical propagation = 0°). Note in Figure 4 how the amplitudes across certain frequency ranges are actually reinforced while other frequency ranges correspond to significant attenuation.

At the receiver location, the receiver wavefield scattered upwards from the earth is recorded at a receiver location as two versions—a version that propagated directly from the earth to the receiver (the up-going wavefield) and a time-delayed version (the down-going wavefield or receiver-side ghost) that is reflected from the free-surface of the ocean with opposite polarity. Again, the frequency-dependent ghost spectra can be described by Figure 4, and the periodic peaks and notches in the amplitude spectrum move to higher values as the emergence angle on the receiver side increases (vertical propagation = 0°). Note that if the effects of both the source-side and receiver-side ghosts are involved the ghost functions will be convolved and the effects in Figure 4 will be exaggerated.

Note in Figure 4 how there is always a notch at 0 Hz for any source or receiver depth, and, therefore, the ultra-low frequency amplitudes will always be penalised by both the source-side and receiver-side ghost effects for conventional source and streamer depths (typically 5–12 m for source arrays and 5–50 m for various streamer configurations). Removal of either/both the source-side and receiver-side ghost effects will evidently allow the recovery of ultra-low frequency amplitudes penalised by ghosting. Parkes and Hegna (2011) and Hegna and Parkes (2012) describe a solution to complete ghost removal that is AVA/AVO-compliant (amplitude vs angle or offset), and phase-compliant for all scenarios of interest to seismic inversion and quantitative interpretation (discussed later). Figure 5 illustrates the ultra-low frequency benefits to seismic images after complete ghost removal.

Three key factors govern the low-end frequency response of seismic data:

1. The effects of the source-side and receiver-side ghosts (discussed above);
2. the cumulative low-cut filter response of the entire acquisition system (recording instrument plus sensor and streamer impedances); and,

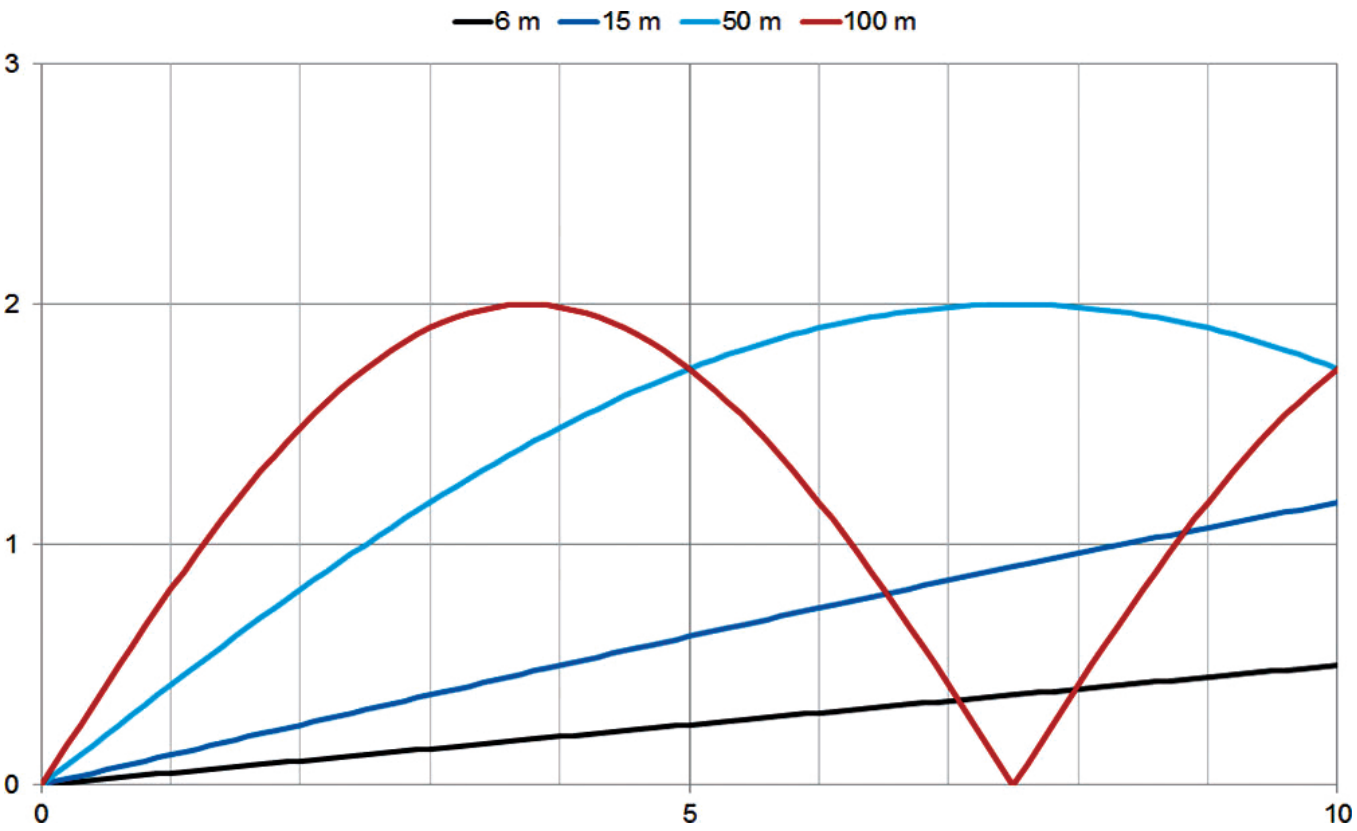

Figure 4. Modelled ghost function spectra for source or receiver depths of 6, 15, 50 and 100 m, respectively. The amplitude scale assumes the ghost-free data has amplitude of one for all frequencies. The ghost creates a frequency-dependent destructive or constructive interference so the amplitude at any given frequency varies between zero (complete cancellation, a notch) or two (perfect reinforcement, a peak). These results assume vertical propagation in the water column, which for a source-side ghost would mean a source emission angle of 0° and for a receiver-side ghost would mean an emergence angle of 0°. Note that as source emission or emergence angle increases all spectra will be stretched towards higher frequency values.

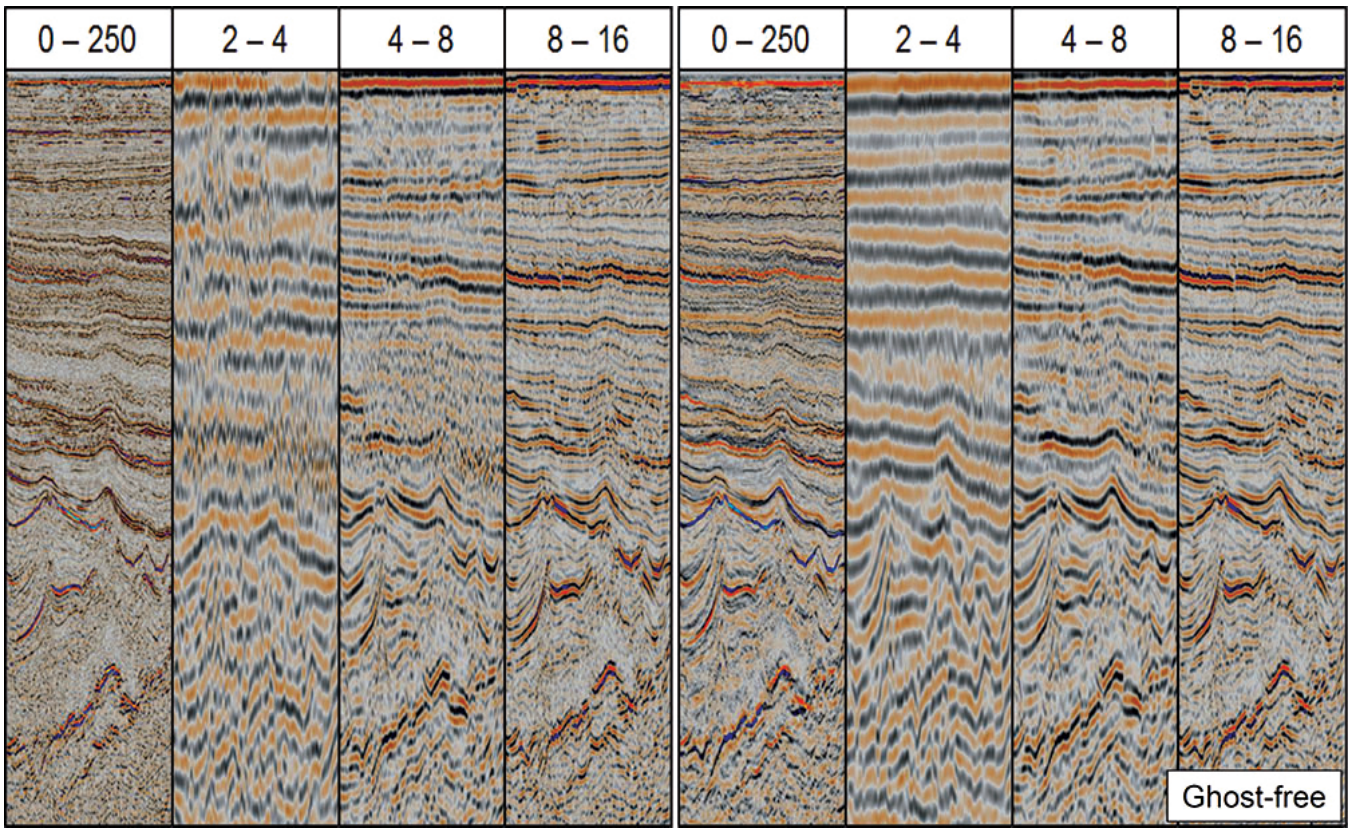

Figure 5. Frequency-limited stack panels displayed with octave ranges for conventional seismic data (left, contains both the source-side and receiver-side ghost effects) versus ghost-free seismic data (right). Two observations are made: Firstly, the 2–4 Hz and 4–8 Hz amplitudes are stronger and the events are more coherent on the right, but secondly, the signal-to-noise content and overall event amplitudes are still much less below 8 Hz for both cases.

3. the ultra-low frequency output of the source array (discussed below).

With regard to the ultra-low frequency output of the source array, note how the signal-to-noise content and overall event amplitudes in the 2–4 Hz and 4–8 Hz panels of Figure 4 are much less than for amplitudes above 8 Hz, even when all ghost effects have been removed. But before we address the physics governing ultra-low frequency output of air gun arrays we will showcase the benefits to quantitative interpretation (QI) of deghosted seismic data.

RECOVERING ELASTIC IMPEDANCES FROM SEISMIC INVERSION

Seismic inversion converts the seismic data from units of reflection amplitude or reflectivity (an interface-related property) to units of elastic impedance (a layer-related property). Pre-stack simultaneous seismic inversion simultaneously inverts for P- and S-impedance and density (highly dependent on the maximum angle of incidence for each two-way time, and, more importantly, the signal-to-noise content of the ultra-far angle stack) at every trace location using any number of input seismic angle stacks. The inversion quantifies the rock properties that result in the observed AVA present in the pre-stack seismic data.

So how does the inversion algorithm work? Although various inversion schemes exist, the commonly used sparse spike inversion is a model-driven inversion that assumes the reflectivity can be thought of as a series of large spikes embedded in a background of small spikes (i.e., assume a Poisson–Gauss probability distribution). Sparse spike inversion assumes that only the large spikes are meaningful. Sparse spike inversion seeks the simplest possible reflectivity model (the minimum number of acoustic impedance interfaces, or spikes) that, when convolved with a wavelet, produces a synthetic that matches the input seismic. The reflectivity sequence is built up one spike at a time. As the band-limited nature of seismic data lacks useful ultra-low frequency components for the derivation of the absolute elastic properties (discussed below), a low-frequency model (LFM) is built to fill the gap in the seismic bandwidth at the ultra-low end of the spectra. The LFM is constructed with the following general characteristics:

- It has a stable, long-wavelength background trend defined using the wells and other available information. The background trend is a stable, long-wavelength solution in the form of a polynomial function of geologically meaningful and measurable quantities. This function is derived using the known well data information, and the quantities may include velocity information, seismic horizons (geobodies), depth of burial, water bottom variations or any other available data deemed likely to influence variations in the particular LFM.
- It ties the well data. This is accomplished by enforcing geophysically and geologically constrained geostatistics that use all available information deemed appropriate (such as the depth calibrated velocity model, seismic horizons and, obviously, well data).

Typical inputs to LFM building may include upscaled (low-frequency) well logs, seismic horizons with associated stratigraphic conformability constraints, rock physics models and velocity models (see later). In fact, any three-dimensional trend term that is expected to correlate with the background model can be used/tested as a constraint—for example, geobodies (defined by seismic horizons) or depth-based trend terms (such as depth below water bottom). Significant pre-stack seismic data and interpretation quality control (QC) is part of the early seismic inversion workflow. Rock physics models can be used to control variation away from well control if desired. Note the emphasis upon establishing low-frequency trends. What we seek is a structurally accurate vehicle to extrapolate calibrated low-frequency impedance information large distances away from available well locations.

The seismic data is modelled as a convolution of the inverted reflection coefficient series with the derived wavelets. A numerical AVA approximation (Zoeppritz approximation) is used to constrain the inverted AVA coefficients and,therefore, the resultant reflectivity and elastic parameters. The results of the simultaneous inversion can be quantitatively integrated with statistical rock physics and stochastic modelling workflows for the purpose of lithology and fluid prediction.

Figure 6 illustrates how a LFM built from seismic velocities, available well log data and other relevant geological information is a necessary complement during absolute seismic inversion. The ultra-low frequency information provided by the LFM is referred to as the low frequency gap, which is typically between 1–7 Hz (or higher with some conventional towed streamer seismic datasets). Even in reasonably explored areas, well locations are typically very sparse, or clustered in a small area of the block/license, and well log data only exists in very limited depth intervals (maybe only the target reservoir interval). The LFM, therefore, typically involves gross interpolation of ultra-low frequency information. Three-dimensional seismic data provides continuous and uniform spatial information about the subsurface, although the high-frequency content decays with increasing depth due to the anelastic attenuation phenomena. In an ideal scenario, elastic seismic inversion would derive full bandwidth information down to 0 Hz from the seismic data through high-resolution velocity models and broadband seismic amplitude data.

ELASTIC INVERSION EXAMPLES WITH LIMITED ULTRA-LOW FREQUENCY CONTENT

Reiser (2012a, b, c) presents a variety of pre-stack simultaneous seismic inversion case studies that showcase the value of deghosted seismic data, with accurate pre-stack amplitude vs angle (AVA) and phase control.

Figure 7 shows dual-sensor streamer data acquired above the Jotun gas field in the Norwegian North Sea. Wavefield separation processing (Carlson et al, 2007) removed the receiver-side ghost effects, increasing the ultra-low frequency amplitude content by an additional octave, while also increasing the high-frequency content. A conventional source array was used, and no effort was made in processing to address the source-side ghost effects. A relative pre-stack simultaneous inversion produced the P-impedance result in the lower part of Figure 7. A simple transform was then applied to convert the relative P-impedance values to absolute P-impedances. This demonstrated an outstanding tie to the P-impedances computed from the well logs, both for quantitative accuracy and vertical resolution (Fig. 8)—without any well information contributing to the LFM.

In the Jotun field examples of Figures 7 and 8, the calibration to absolute P-impedance was proven to be robust away from the well location, assisted by the fact that the structural trends are gentle in this area and the material properties of the earth are homogeneous across large distances. This example suggests that receiver-side deghosting that preserves pre-stack AVA-compliance and phase-compliance is a robust platform for elastic seismic inversion, and, more importantly, can be used with confidence for the identification of leads and the de-risking of prospects.

The structural trends in the Frigg gas field are more locally variable than the Jotun field roughly 50 km to the south. Reservoir depth is at roughly 2 km in an Eocene deep-marine environment. Production has ceased and the field is considered to be depleted.

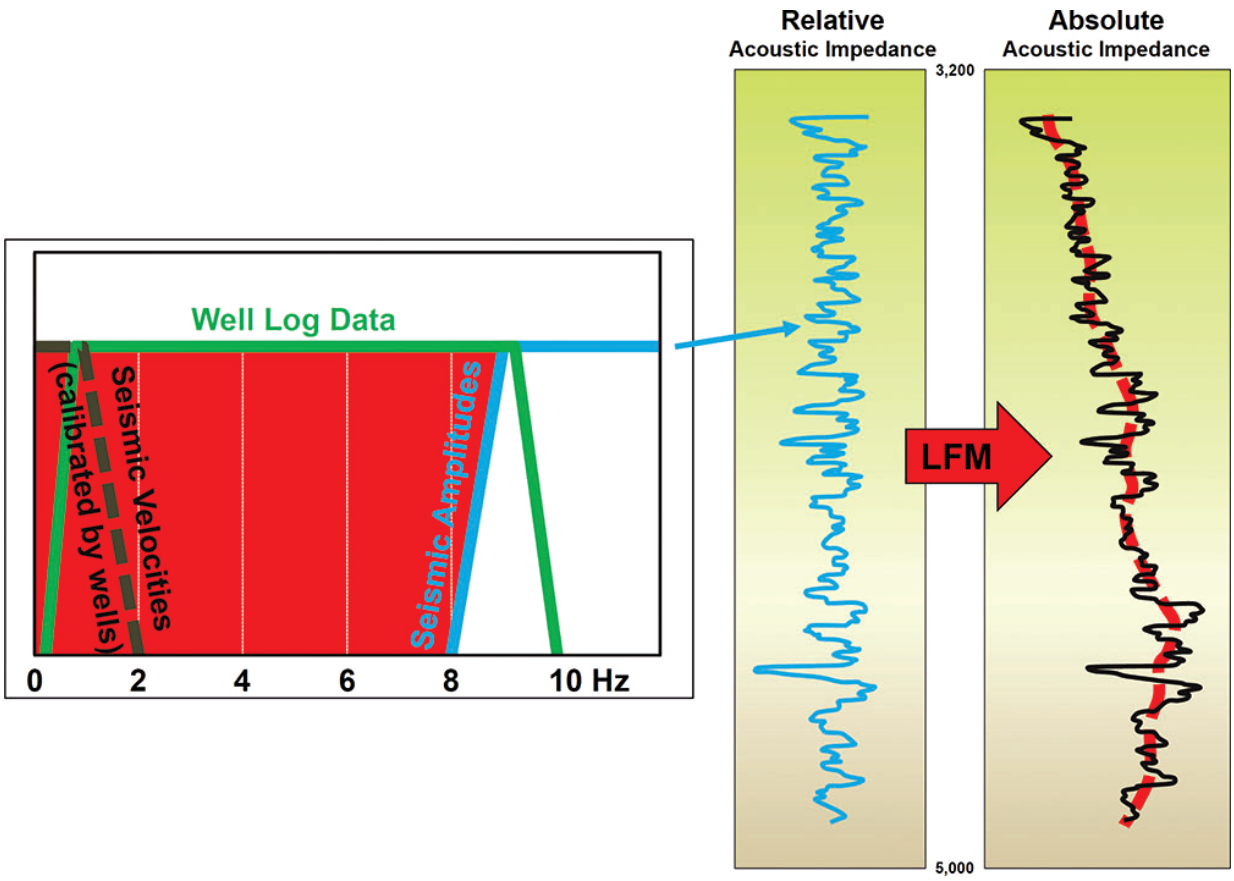

Figure 6. Schematic illustration of the three frequency-dependent contributions to seismic inversion: the velocity model (typically 0–1 Hz), available well log data and other relevant structural trend information (the LFM), and the seismic amplitudes (typically frequencies no less than about 7 Hz). Relative inversion with only the seismic amplitude data cannot recover accurate absolute estimates of P-impedance or S-impedance. Elastic impedances can be accurately estimated only when the low frequency background trend from the LFM is included in the inversion.

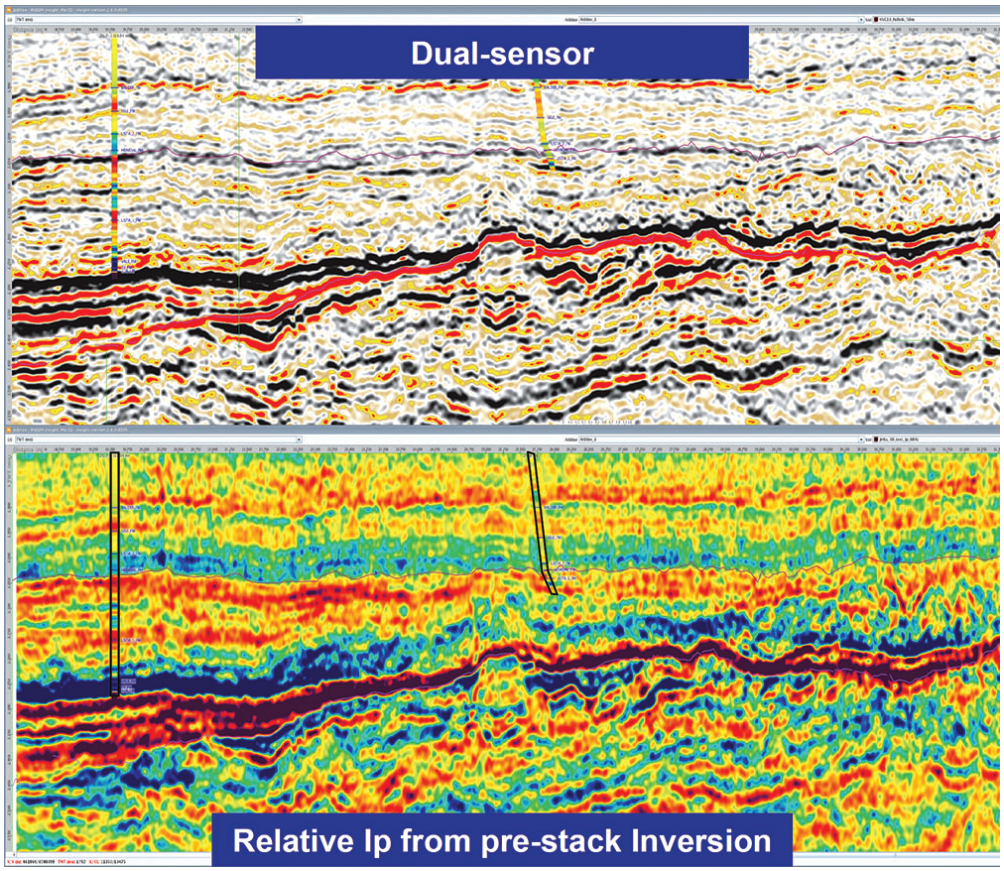

Figure 7. Seismic amplitude image (upper) and P-impedance image (lower) through the Jotun gas field. Two well trajectories are plotted in the upper panel, with colour scale corresponding to P-impedance computed from the well logs and filtered to the seismic bandwidth. Refer also to Figure 8.

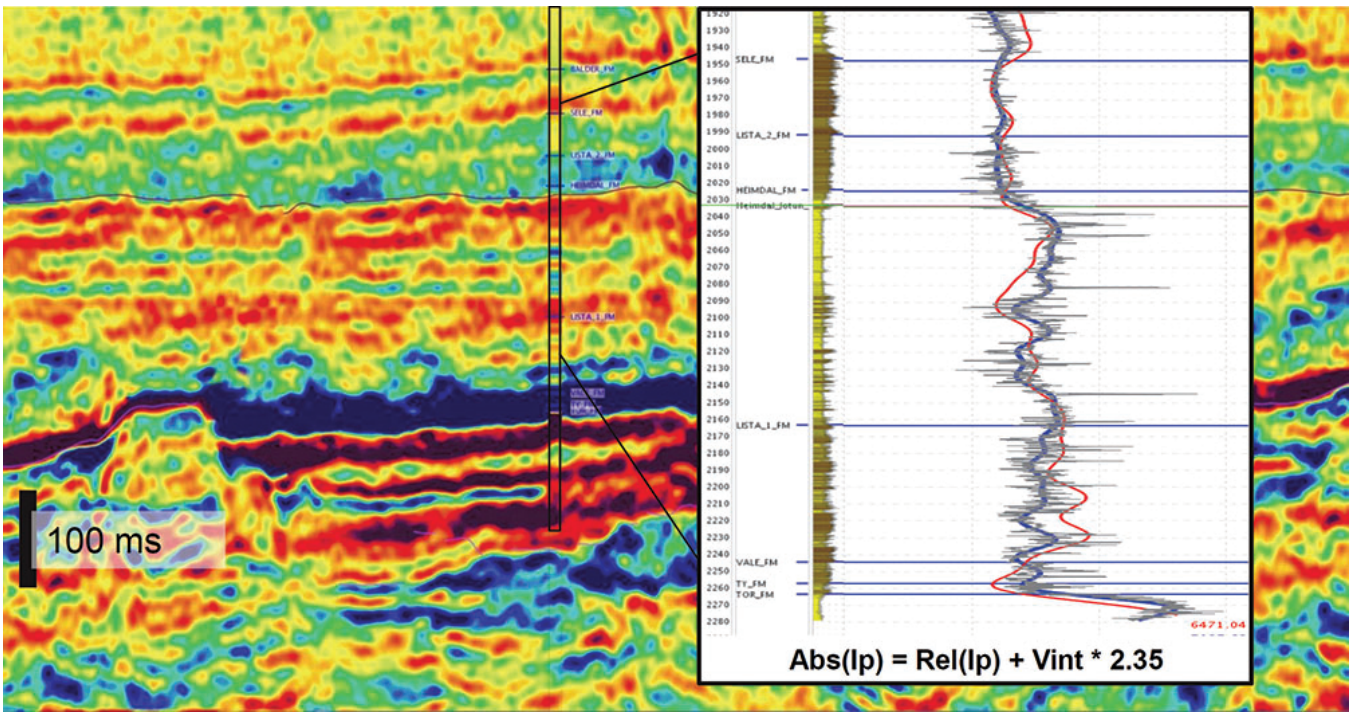

Figure 8. Zoom of the relative P-impedance image in Figure 7. The right panel shows the gamma ray log recorded at kHz frequencies. The P-impedance computed from the well logs has been filtered to the seismic bandwidth (blue curve). The relative P-impedance inverted from the band-limited seismic data has been transformed to an absolute P-impedance profile using the simple arithmetic operation in red font: the sum of relative P-impedance and the interval velocity multiplied by a constant density of 2.35 g/cm^3.

Figure 9 compares absolute pre-stack seismic inversion results for conventional vs dual-sensor three dimensional streamer data, the difference again being receiver-side wavefield separation and deghosting for the latter dataset. The same 0–5 Hz LFM was used during the inversion of both datasets. The differences between the two results are compelling. The dual-sensor pre-stack inversion result clearly delineates a gas-water contact (GWC) on the vertical section, which is absent and/or contaminated by the strong sidelobe amplitudes on the conventional inversion result. The geometry of sandstone channels is far less ambiguous in the dual-sensor inversion result; residual gas accumulations become clearly delineated, and the vertical and spatial resolution of various lithology classes is significantly improved. There is uplift on various fronts: Improved interpretability; sharper reservoir delineation; and, the potential mapping of remaining gas accumulations.

Three key conclusions can be made from the results in Figure 9:

1. Whereas conventional seismic data lacks ultra-low frequency amplitude information below at least 7 Hz (typically closer to 10 Hz), the dual-sensor seismic data after receiver-side deghosting contain useful amplitude information down to at least 5 Hz;
2. the low-frequency gap between 5 Hz in the LFM and the lowest significant frequency in the conventional data corrupts the clarity of the inversion result in the upper panel of Figure 9. In comparison, no such low-frequency gap exists in the result shown in the lower panel of Figure 9; and,
3. the wavefield separation processing applied to dual-sensor streamer data yields high signal-to-noise pre-stack data that accurately preserved the AVA and phase information.

Note, however, that the dual-sensor streamer data in the lower panel of Figure 9 still lacks ultra-low frequency amplitude content below about 5 Hz because of the aforementioned effects of the source-side ghost, the cumulative lo-cut filter response of the entire acquisition system, and the ultra-low frequency output of the source array. The frequency panels in Figure 5 illustrate that even in a fully ghost-free scenario the amplitude content has rolled off significantly below about 4 Hz. The paper now discusses the physics of the ultra-low frequency output of air guns and air gun arrays.

FIGHTING THE INESCAPABLE LAWS OF PHYSICS

The low-frequency spectral characteristics of signals emitted from marine air gun arrays are constrained by the source-side ghost effects (discussed earlier), the response of the air guns, and the air gun array design. Hegna and Parkes (2011) refer to the Rayleigh-Willis equation, which describes a proportional relationship between the bubble oscillation period from an air gun and the cube root of the air gun volume. A longer bubble period equates to lower characteristic frequency, with the frequency corresponding to the most significant low-end amplitude (Fig. 10). The use of air guns significantly larger than those used in the industry today (typically no larger than 250 in^3) is impractical as the associated bubble behavior is too large and chaotic to allow modelling or in-field measurement of the far-field signatures in any accurate manner. This means that ultra-low frequency amplitude and phase control would be impossible in seismic processing and/or inversion. Hegna and Parkes (2011) also demonstrate that the bubble oscillation period gets shorter with increasing hydrostatic pressure and, hence, increasing tow depth. For a particular gun volume and pressure, therefore, the power of the signals in the ultra-low frequency end emitted by an air-gun decrease with increasing tow depth. While a number of source array configurations with sub-arrays deployed at different depths (multi-level sources, MLS) have emerged in recent years, it is noted that none reduce the characteristic frequencies of the constituent air guns. MLS configurations can attenuate the source-side ghost note and bias the overall source energy to specific frequency bands, but none improve ultra-low frequency output. One published research and development exception (Hopperstad et al, 2012) arranged six guns in a tight cluster, so that even if the guns were of different sizes, their oscillating bubbles will assume a synchronised oscillation (frequency locking).

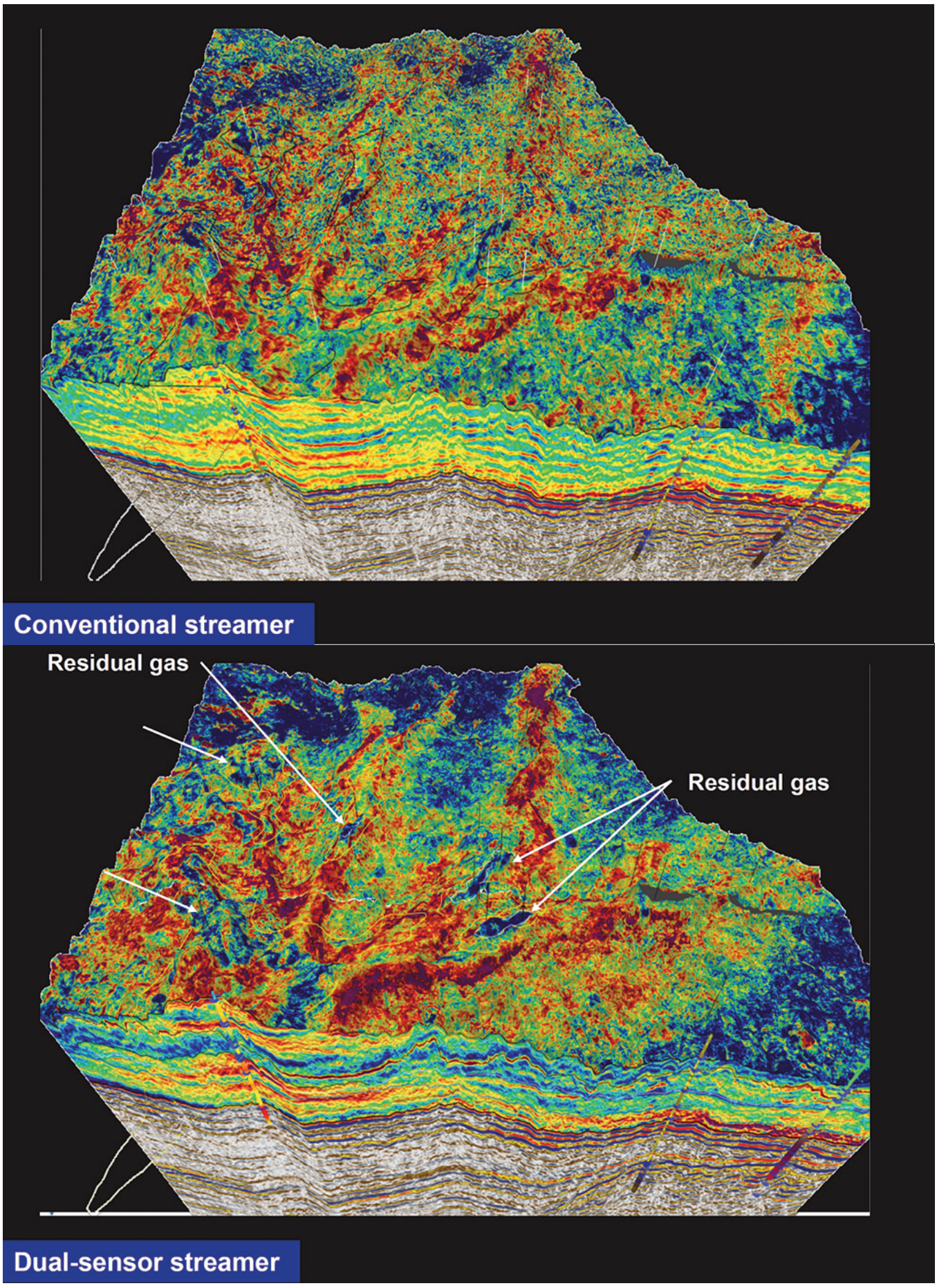

Figure 9. Comparison of absolute inversion results with the same 0–5 Hz LFM for conventional (upper) vs dual-sensor (lower) three-dimensional seismic data over the Frigg gas field.

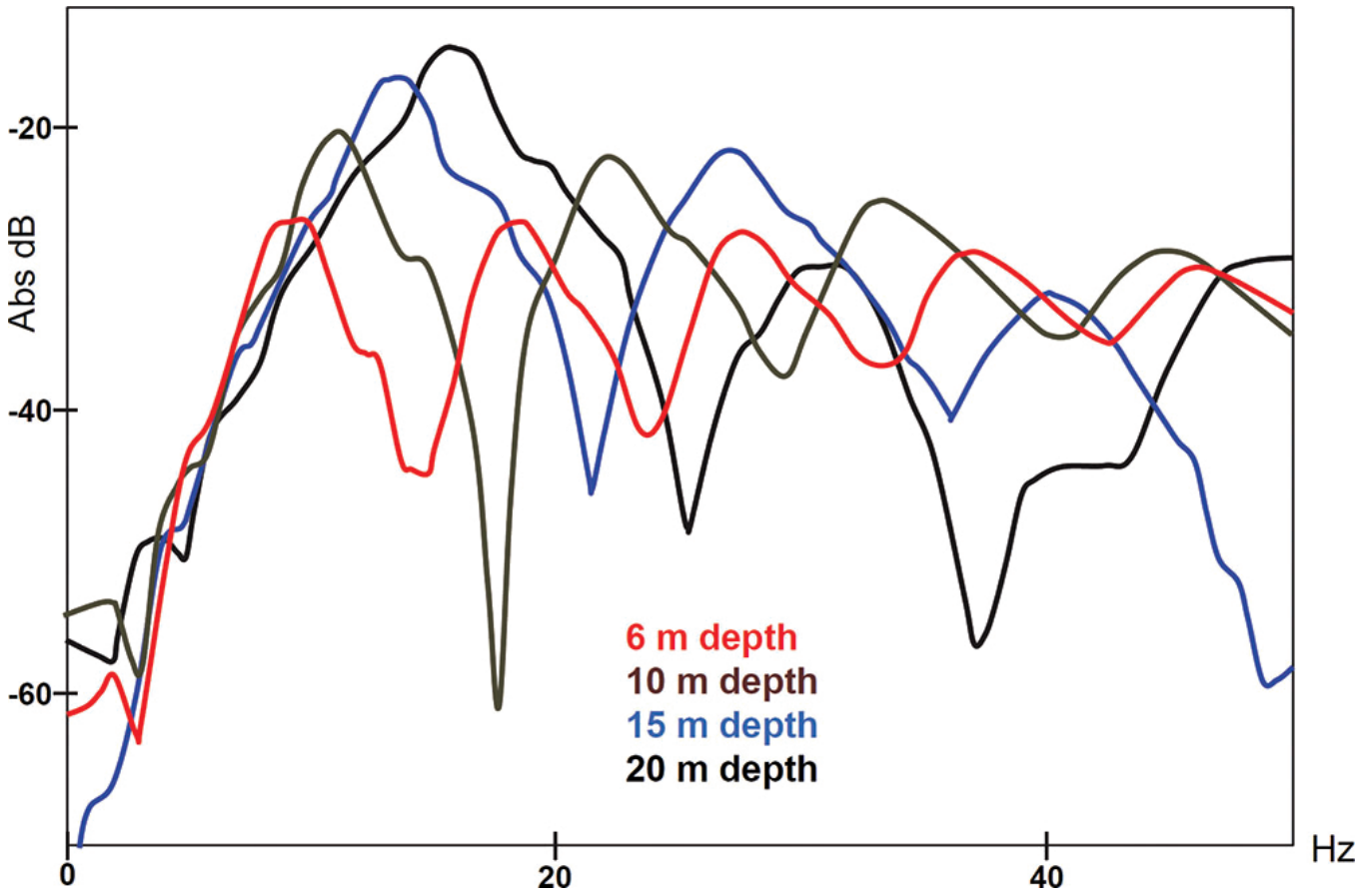

Figure 10. Amplitude spectra for a 250 in^3 air gun fired at 2,000 psi and different depths. The frequency corresponding to the first significant amplitude (the characteristic frequency) actually moves to higher values as air gun depth increases.

Conventional-size air guns, therefore, might be arranged such that each of their bubbles behaves somewhat like the bubble of one huge air gun—with a longer bubble period and improved low frequency output. A trial resulted in a characteristic frequency of about 5 Hz, but with about -10 dB power reduction compared to the characteristic frequency from a conventionally configured arrangement of the same six air guns.

As an alternative consideration to air guns, Figure 11 shows a schematic representation of a prototype deep-towed marine vibrator designed to output ultra-low frequencies in the range of 2–6 Hz with comparable power to a conventional air gun array. Based on established towed marine vibrator technology (Tenghamn, 2006), the design is towed very deep (50–120 m) to exploit the source-side ghost effect across the frequency range of interest. Such an approach would necessitate combined processing of impulsive air gun array shots and transient marine vibrator sweeps.

Overall, there exists no commercialised impulsive (e.g., air gun) or transient (e.g., towed marine vibrator) source solution to significantly improve the ultra-low frequency (0–7 Hz) output of seismic sources, for any source geometry or configuration, towing depth or firing scheme. The ultra-low frequency component of the broadband seismic story is, therefore, constrained to removing the effects of the source-side and receiver-side ghosts (recovering more low-frequencies from the earth, as opposed to injecting more low-frequencies into the earth).

REMOVING THE LOW-FREQUENCY GAP BY BUILDING GEOLOGICALLY-CONSISTENT VELOCITY MODELS

Earlier discussion noted that the LFM used in seismic inversion describes a stable long-wavelength background trend that is a long-wavelength solution in the form of a polynomial function of geologically meaningful and measurable quantities, and will tie available well data. What we seek is a structurally accurate vehicle to extrapolate calibrated low frequency impedance information large distances away from available well locations.

Full-waveform inversion (FWI) is an iterative imaging and inversion technique that seeks to find a high-resolution, high-fidelity model of the subsurface that is capable of matching individual seismic waveforms in an original raw field data set, trace by trace. FWI is most commonly used to recover high-resolution P-wave velocity models within heterogeneous overburden above deeper reservoirs. These shallow velocity models are then combined with conventional pre-stack depth migration (PSDM) to improve the imaging of the underlying reservoir using sub-critical reflection data. FWI also promises to be a powerful vehicle to complement or supplement LFM building pursuits, and to greatly reduce the traditional dependence upon non-seismic sources of information.

The spatial resolution and complexity of the FWI-recovered velocity model often require that a high-fidelity PSDM scheme is used for the migration—typically, this will be a reverse-time migration (RTM) scheme based on the full two-way wave equation. FWI typically uses wide-angle refracted arrivals to build its velocity model, although reflection-based FWI solutions are emerging in the industry. Refraction-based FWI is mainly driven by diving waves, wavefronts continuously refracted downwards and then upwards through the earth due to the presence of a vertical velocity gradient. The nature of diving wave propagation usually means that only shallow velocity model updates are possible for standard streamer lengths. A benefit is that minimum pre-processing is required and multiples can be left in the data. In contrast, reflection-based FWI has the benefits that much deeper velocity model updates are possible for standard streamer lengths, but the input data should have deghosting and shallow water demultiple applied first during pre-processing.

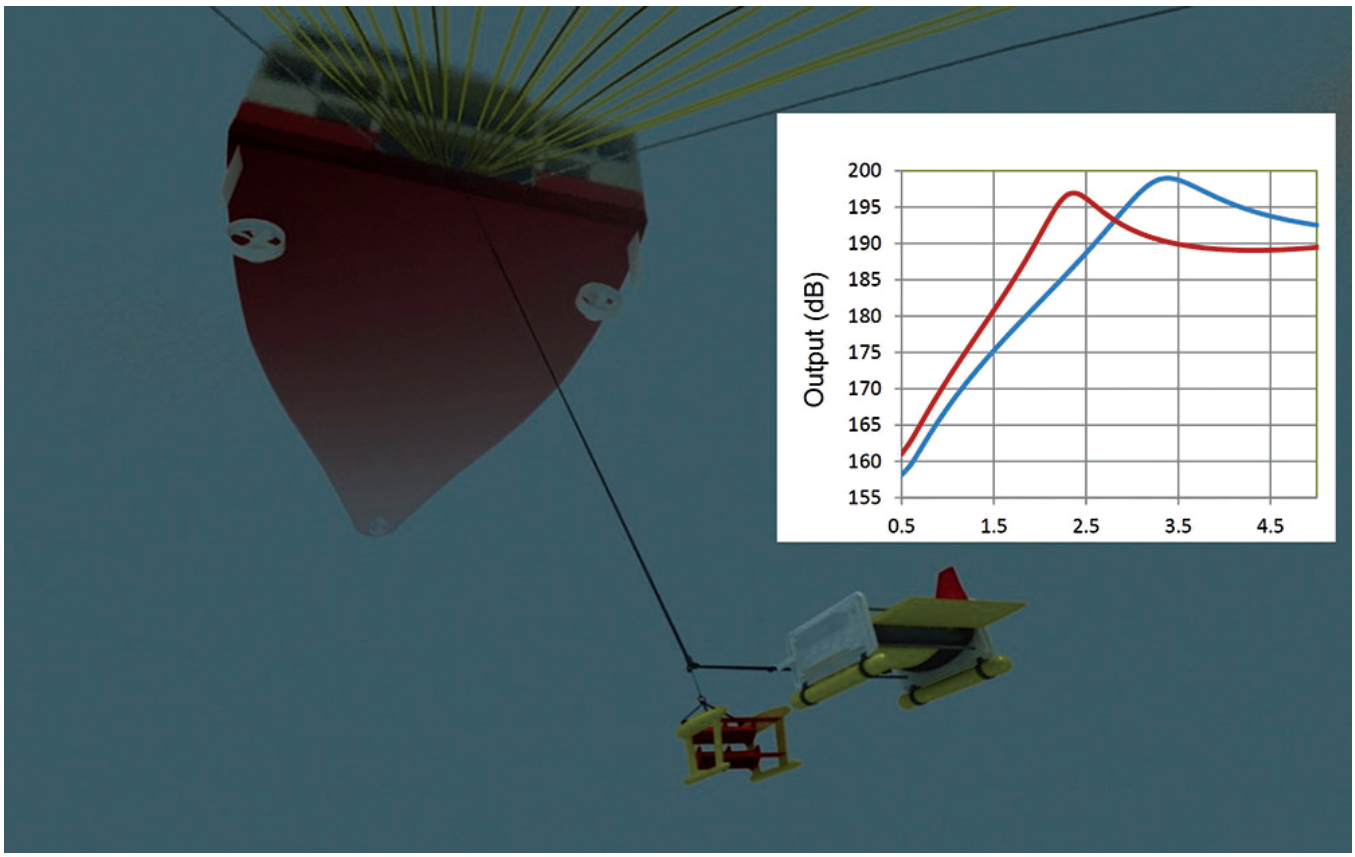

Figure 11. Schematic illustration of a large towed marine vibrator (50–100 m depth). A towing depth between 50–100 m will yield a peak source-side ghost response between about 3–8 Hz. Two possible output spectra on the right are derived from finite element modelling.

FWI is ideally suited to broadband seismic data particularly rich in ultra-low frequency amplitude information (e.g., down to at least 5 Hz), otherwise so-called cycle skipping problems will translate to artifacts in the estimated velocity model (Virieux and Operto, 2009). To be technically strict, the input data should be rich in low wavenumber information, implying the availability of extremely long offsets—longer than those likely to be used in typical processing and imaging. Having more ultra-low frequency amplitudes available will help mitigate the FWI requirement for very long offsets. Because FWI honours the physics of wave propagation, its spatial resolution is limited only by the source and receiver distribution, the noise level, and the local seismic wavelength. In contrast, methods that are based upon travel times (e.g., tomography), and, therefore, implicitly upon simplified wave propagation, have a spatial resolution that is limited also by the size of the local Fresnel zone. In practice, this means that FWI models are almost always better spatially resolved than equivalent models generated by more conventional methods.

Figure 12 shows the significant detail added to the velocity model from fully deghosted data acquired in the Møre Margin area of the Norwegian North Sea, using a reflection-based FWI (Ramos-Martinez et al, 2013). The maximum offset is 10,050 m. Preprocessing steps included noise-attenuation, source- and receiver-side deghosting, and multiple attenuation. Coherent (albeit weak) reflected events are observed in the deghosted data at frequencies lower than 3 Hz. As evident in Figure 12, a mute was applied before FWI to remove water bottom, diving wave and refraction events, while retaining as many post-critical reflection events as possible. The starting depth velocity model was built using conventional tomography. Overall, the results testify to the benefits of ghost-free data as the optimum platform for reflection-based FWI. An industry rule-of-thumb is that refraction-based FWI can deliver FWI velocity model information to a maximum depth equivalent to one-third of the maximum offset. In contrast, the results in Figure 12 suggest that this increases to about one-half of the maximum offset when reflection-based FWI is used.

The left side of Figure 13 shows superimposed amplitude spectra for the starting and final FWI depth velocity models in Figure 12. As is traditionally the case, the velocity model output from tomography only provides very long wavelength structural information in the range of 0–1 Hz. In contrast, the FWI velocity model provides structural information up to at least 6 Hz. The right side of Figure 13 schematically illustrates where the content of the discussion here is leading. Increased resolution in the velocity model provided by FWI promises to improve velocity-based structural information from 0–1 Hz to maybe 0–6 Hz (or more). Improved ultra-low frequency bandwidth provided by deghosting promises to improve ultra-low frequency amplitude content down to at least 6 Hz. The traditional low frequency gap confronting relative elastic seismic inversion has, therefore, been closed from both sides.

Note the model proposed in the right side of Figure 13 does not preclude the contribution of well log calibrations where available for seismic inversion. As demonstrated in Figures 7 and 8, it may be possible to extrapolate impedance information large distances away from well locations in favorable geological settings using relative seismic inversion results calibrated with simple transforms to absolute impedance estimates. It is expected with the assistance of the developments described here that such transforms will be robustly established even when the geological structure and properties vary laterally away from the wells (refer also to Figure 14). This is the ultimate vision for seismic inversion—deriving all impedance information only from the seismic data, exploiting the three-dimensional spatial information to yield three-dimensional spatially accurate elastic impedance estimates.

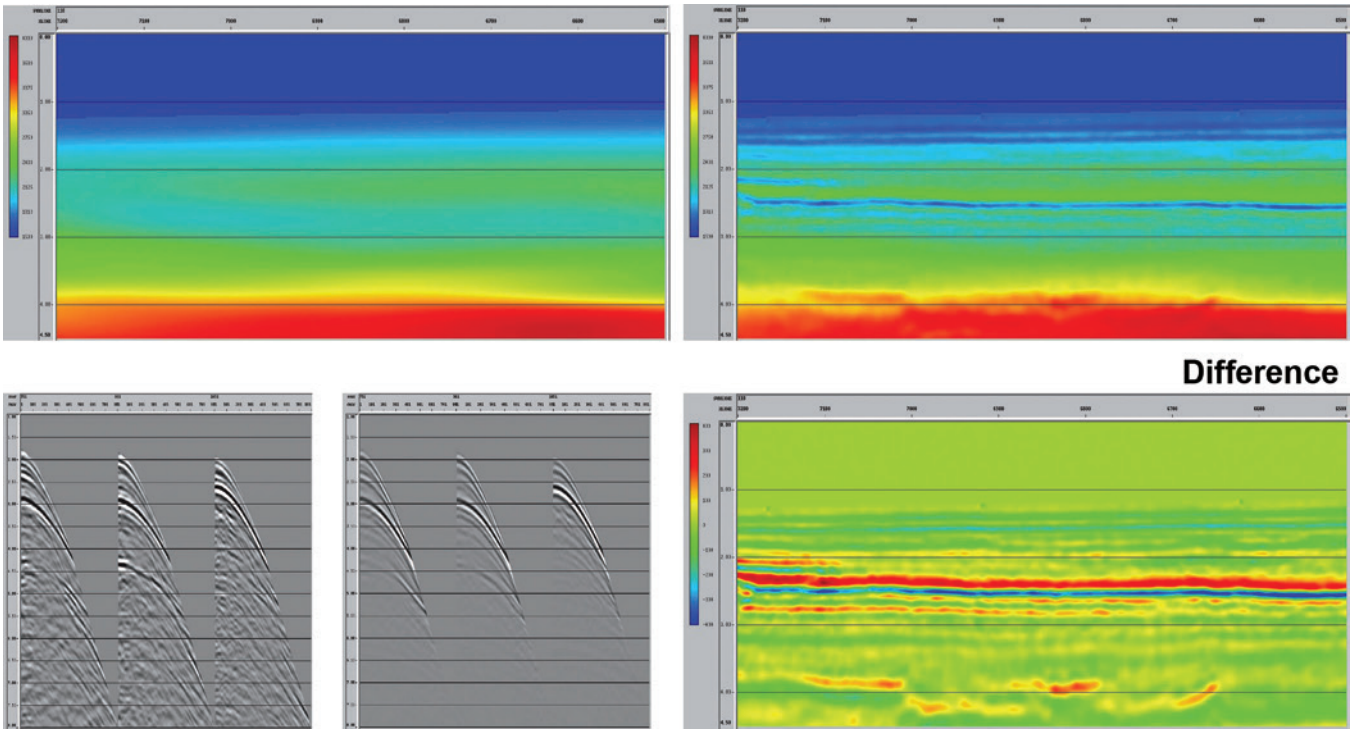

Figure 12. The two greyscale images in the lower row show example shot gathers after a surgical mute is applied to eliminate the water bottom reflection for field data (left), and the modeled data with the final FWI velocity model (right). The upper left shows the starting velocity model for the inversion and output from conventional tomographic depth velocity model building. The upper right panel shows the inverted velocity model after FWI. The lower right panel shows the difference (the additional detail introduced) in the velocity model achieved by FWI. The vertical axis on the velocity models is depth in km (0–4.5 km), and the horizontal axis is cross-line number with a total length of 17.5 km. From Ramos-Martinez et al (2013).

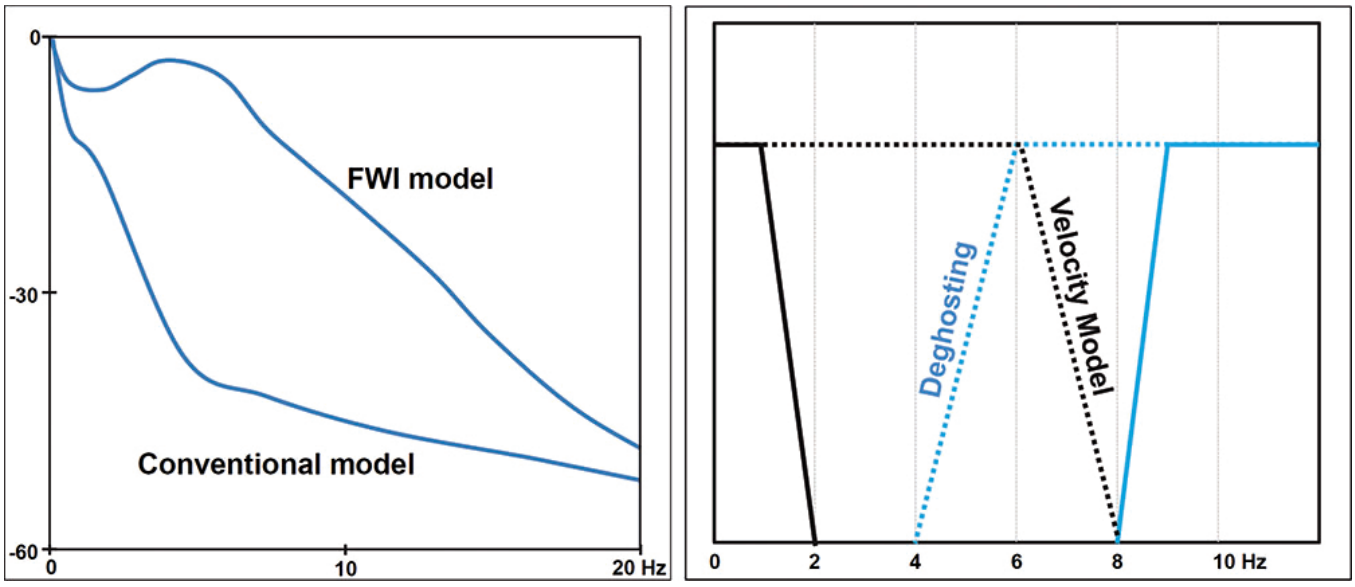

Figure 13. The left panel shows superimposed spectra for the starting and final FWI depth velocity models in Figure 12. The horizontal scale is 0–20 Hz. The right panel shows a schematic illustration of how increased resolution in the velocity model provided by FWI and improved low frequency bandwidth provided by deghosting promises to remove the traditional low-frequency gap confronting relative elastic seismic inversion.

SUMMARY

Towed streamer seismic data is, by nature, band-limited and, therefore, yields poor vertical resolution for interpretation, and prohibits seismic inversion from yielding a quantitatively accurate understanding of the reservoir. The elusive ultra-low frequency range of interest is about 1–7 Hz. Conventional seismic sources cannot produce significant amplitudes in this frequency range, irrespective of the air gun array configuration or towing depth. While removal of the source-side and receiver-side ghost effects recovers ultra-low frequency amplitudes penalised by seismic wavefield interference from the free-surface of the ocean, we can never recover more ultra-low frequency content than was injected into the earth in the first place.

A workflow is described, however, wherein the well-known low-frequency gap is mitigated from the low-end frequency side by building high-resolution and geologically-consistent detail into seismic velocity models through the process of full waveform inversion (FWI), notably reflection-based FWI. In concert, deghosting promises to improve ultra-low frequency seismic amplitude content down to at least 6 Hz. The traditional low frequency gap confronting relative elastic seismic inversion has, therefore, been closed from both sides. It

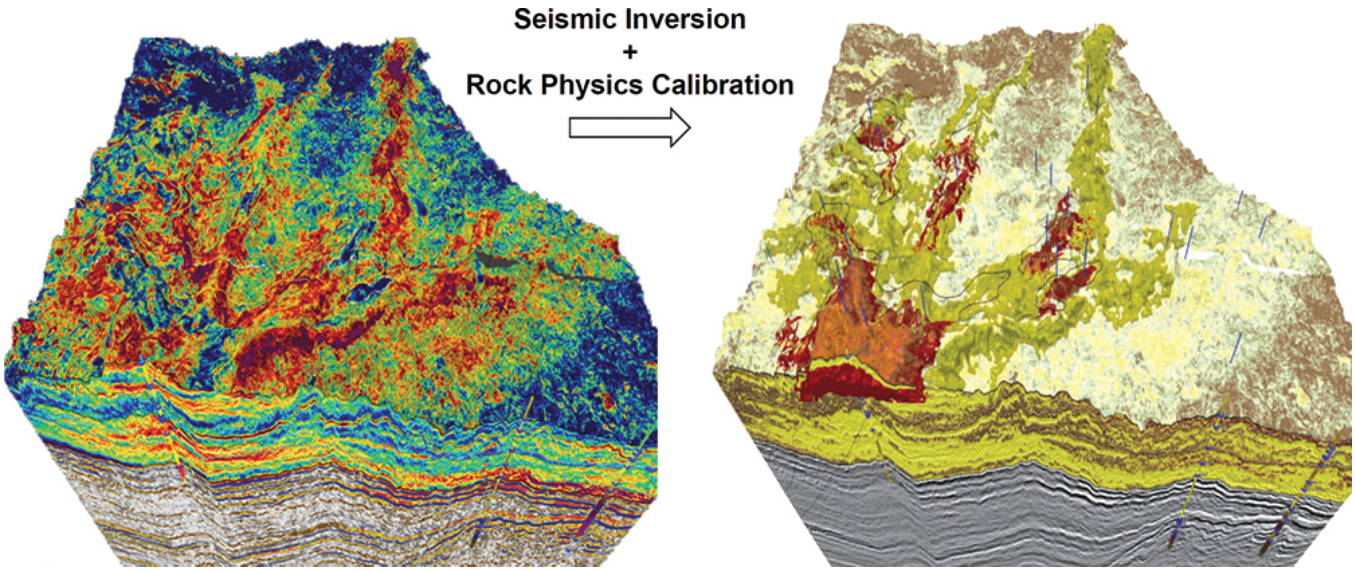

Figure 14. The right panel shows the predicted lithology based upon the pre-stack inversion of dual-sensor seismic data acquired over the Frigg gas field (left, and Figure 9) calibrated by depth-dependent rock physics modelling. As the amount of ultra-low frequency information derivable from the seismic velocity and amplitude information is improved, the dependence upon well information for building the LFM will decrease.

is expected, with the assistance of the developments described here, that accurate transforms from relative to absolute elastic impedances can be robustly established, even when the geological structure and properties vary laterally away from the wells. This is the ultimate vision for seismic inversion—deriving all impedance information only from the seismic data, exploiting the three-dimensional spatial information to yield three-dimensional spatially accurate elastic impedance estimates. The pursuits discussed in this paper aim to efficiently facilitate quantitative reservoir description with less uncertainty, leading to faster and more robust reserves evaluation.

REFERENCES

CARLSON, D., LONG, A., SÖLLNER, W., TABTI, H., TENGHAMN, R. AND LUNDE, N., 2007—Increased resolution and penetration from a towed dual-sensor streamer. In: First Break, 26 (12), 71–77.

HEGNA, S. AND PARKES, G., 2011—The low frequency output of marine air-gun arrays. Society of Exploration Geophysicists 81st Annual Meeting, San Antonio, Texas, 18–23 September.

HEGNA, S. AND PARKES, G., 2012—The principle of using complementary acquisition components to achieve broadband seismic. Society of Exploration Geophysicists 82nd Annual Meeting, Las Vegas, Nevada, 4–9 November.

HOPPERSTAD, J.F., LAWS, R. AND KRAGH, E., 2012—Hypercluster of airguns – More low frequencies for the same quantity of air. European Association of Geoscientists and Engineers 74th Conference & Exhibition, Copenhagen, Denmark, 4 June, Z011.

PARKES, G. AND HEGNA, S., 2011—An acquisition system that extracts the earth response from seismic data. In: First Break, 29 (12), 31–37.

RAMOS-MARTINEZ, J., ZOU, Z., KELLY, K. AND TSIMELZON, B., 2013—Reflection FWI from fully deghosted towed-streamer data: A field data example. Society of Exploration Geophysicists 83rd Annual Meeting, Houston, Texas, 22–27 September, 887–891

REISER, C., ENGELMARK, F. AND ANDERSON, E., 2012a—Broadband seismic reviewed for the end-user benefits in interpretation and reservoir geophysics. European Association of Geoscientists and Engineers 74th Conference & Exhibition, Copenhagen, Denmark, 4 June, B030.

REISER, C., ENGELMARK, F., ANDERSON, E. AND BIRD, T., 2012b—Value of the broadband seismic for interpreter and reservoir geophysics. European Association of Geoscientists and Engineers 74th Conference & Exhibition, Copenhagen, Denmark, 18 March, J06.

REISER, C., BIRD, T., ENGELMARK, F., ANDERSON, E. AND BALABEKOV, Y., 2012c—Value of broadband seismic for interpretation, reservoir characterization and quantitative interpretation workflows. In: First Break, 30 (9), 67–75.

TEN KROODE, F., BERGLER, S., CORSTEN, C., DE MAAG, J.W., STRIJBOS, F. AND TIJHOF, H., 2013—Broadband seismic data — The importance of low frequencies. In: Geophysics, 78 (2), WA3-WA14.

TENGHAMN, R., 2006—An electrical marine vibrator with a flextensional shell. Australian Society of Exploration Geophysicists 16th Conference & Exhibition. Melbourne, Victoria, December, 1-5.

VIRIEUX, J. AND OPERTO, S., 2009—An overview of full-waveform inversion in exploration geophysics. In: Geophysics, 74 (6), WCC127-WCC152.

Authors' biographies next page.

THE AUTHORS

Andrew Long has a PhD in geology from the University of Western Australia (UWA), and has worked for various service companies and academia for a 20 year period. He is Chief Scientist for Geoscience & Engineering in PGS, having been employed by PGS since 1997. Member: Petroleum Exploration Society of Australia (PESA), Society of Economic Geologists (SEG), European Association of Geoscientists & Engineers (EAGE), Australian Society of Exploration Geophysicissts (ASEG) and South East Asia Petroleum Exploration Society (SEAPEX).

andrew.long@pgs.com

Cyrille Reiser has a Ph.D. in geology from Lyon's Ecole Normale, and has specialized in reservoir characterisation for 15 years. He is Reservoir Characterisation Director for Reservoir Services in PGS, having been employed by PGS since 2008. Cyrille is a member of SEG, EAGE and Petroleum Exploration Society of Great Britain (PESGB).

cyrille.reiser@pgs.com

THIS PAGE LEFT BLANK INTENTIONALLY.